Applied Geochemistry 63 (2015) 58–69

Contents lists available at ScienceDirect

Applied Geochemistry

journal homepage: www.elsevier.com/locate/apgeochem

Topographic controls on the depth distribution of soil CO_2 in a small temperate watershed

Elizabeth A. Hasenmueller [a, *], Lixin Jin [b], Gary E. Stinchcomb [c], Henry Lin [d], Susan L. Brantley [e, f], Jason P. Kaye [d]

[a] Department of Earth & Atmospheric Sciences, Saint Louis University, Saint Louis, MO, USA
[b] Department of Geological Sciences, University of Texas at El Paso, El Paso, TX, USA
[c] Watershed Studies Institute and Department of Geosciences, Murray State University, Murray, KY, USA
[d] Department of Ecosystem Science and Management, The Pennsylvania State University, State College, PA, USA
[e] Department of Geosciences, The Pennsylvania State University, State College, PA, USA
[f] Earth and Environmental Systems Institute, The Pennsylvania State University, State College, PA, USA

ARTICLE INFO

Article history:
Received 24 January 2015
Received in revised form
13 July 2015
Accepted 14 July 2015
Available online 4 August 2015

Keywords:
Carbon dioxide
Soil atmosphere
Topographic position
Chemical weathering
Carbon cycle

ABSTRACT

Accurate measurements of soil CO_2 concentrations (pCO_2) are important for understanding carbonic acid reaction pathways for continental weathering and the global carbon (C) cycle. While there have been many studies of soil pCO_2, most sample or model only one, or at most a few, landscape positions and therefore do not account for complex topography. Here, we test the hypothesis that soil pCO_2 distribution can predictably vary with topographic position. We measured soil pCO_2 at the Susquehanna Shale Hills Critical Zone Observatory (SSHCZO), Pennsylvania, where controls on soil pCO_2 (e.g., depth, texture, porosity, and moisture) vary from ridge tops down to the valley floor, between planar slopes and slopes with convergent flow (i.e., swales), and between north and south-facing aspects. We quantified pCO_2 generally at 0.1–0.2 m depth intervals down to bedrock from 2008 to 2010 and in 2013. Of the variables tested, topographic position along catenas was the best predictor of soil pCO_2 because it controls soil depth, texture, porosity, and moisture, which govern soil CO_2 diffusive fluxes. The highest pCO_2 values were observed in the valley floor and swales where soils are deep ($\geq$0.7 m) and wet, resulting in low CO_2 diffusion through soil profiles. In contrast, the ridge top and planar slope soils have lower pCO_2 because they are shallower ($\leq$0.6 m) and drier, resulting in high CO_2 diffusion through soil profiles. Aspect was a minor predictor of soil pCO_2: the north (i.e., south-facing) swale generally had lower soil moisture content and pCO_2 than its south (i.e., north-facing) counterpart. Seasonally, we observed that while the timing of peak soil pCO_2 was similar across the watershed, the amplitude of the pCO_2 peak was higher in the deep soils due to more variable moisture content. The high pCO_2 observed in the deeper, wetter topographic positions could lower soil porewater pH by up to 1 pH unit compared to porewaters equilibrated with atmospheric CO_2 alone. CO_2 is generally the dominant acid driving weathering in soils: based on our observations, models of chemical weathering and CO_2 dynamics would be improved by including landscape controls on soil pCO_2.

© 2015 Elsevier Ltd. All rights reserved.

1. Introduction

Over geologic time, the dissolution of soil CO_2 into soil porewater or shallow groundwater has provided the major source of acidity for rock weathering. Thus, accurate predictions of soil CO_2 concentrations (pCO_2) are essential for determining bedrock weathering rates (Brantley et al., 2013) and their role in the global carbon (C) cycle (e.g., Berner and Berner, 1996; Williams et al., 2007; Szramek et al., 2007; Beaulieu et al., 2010). At our research watershed in the Susquehanna Shale Hills Critical Zone Observatory (SSHCZO) in central Pennsylvania, results based on water chemistry are consistent with a strong link between soil pCO_2 and weathering. In the top 2 m of regolith, dissolution of silicate minerals (mainly chlorite, Eq. (1), and illite, Eq. (2); see Jin et al., 2010) consumes dissolved CO_2 (Eq. (3)) as evidenced by the ^{13}C of DIC and positive correlations between soil pCO_2 and DIC concentrations in porewaters (Jin et al., 2014). Carbonates in the Silurian Rose Hill

* Corresponding author.
E-mail address: hasenmuellerea@slu.edu (E.A. Hasenmueller).

http://dx.doi.org/10.1016/j.apgeochem.2015.07.005
0883-2927/© 2015 Elsevier Ltd. All rights reserved.

Formation shale, including calcite and ankerite, have been completely weathered out of surface soils.

Chlorite dissolution: $(Fe_{0.24}Mg_{0.38}Al_{0.38})_6(Si_{0.07}Al_{0.93})_4O_{10}(OH)_{8(s)} + 5.72H_4SiO_{4(aq)} + 4.56H^+_{(aq)} \rightarrow 1.44FeOOH_{(s)} + 2.28Mg^{2+}_{(aq)} + 3Al_2Si_2O_5(OH)_{4(s)} + 11H_2O_{(l)}$ (1)

Illite dissolution: $K_{0.77}(Si_{0.30}Al_{0.70})(Fe_{0.48}Mg_{0.07}Al_{0.45})AlSi_3O_{10}(OH)_{2(s)} + 0.91H^+_{(aq)} + 3.235H_2O_{(1)} \rightarrow 0.77K^+_{(aq)} + 0.48FeOOH_{(s)} + 0.07Mg^{2+}_{(aq)} + 1.075Al_2Si_2O_5(OH)_{4(s)} + 1.15H_4SiO_{4(aq)}$ (2)

CO_2 *dissolution* : $CO_{2(g)} + H_2O_{(l)} \rightarrow HCO_3^-(aq) + H^+_{(aq)}$ (3)

Despite pCO_2 at depth acting as a source of acidity, mineral–water reactions buffer porewater pH to higher values as soil depth increases. This is consistent with observations that soils at the SSHCZO exhibit decreasing proportions of Al (compared to base cations Ca and Mg) on soil exchange sites with increasing depth and reduced chlorite and/or illite dissolution with increasing depth (Jin et al., 2010, 2011). Moreover, the alkalinity of porewaters increases downward with increasing extent of rock weathering (i.e., Eqs. (1) and (2)). These preliminary results from a limited number of locations and time points have led us to question how soil pCO_2 varies in space and time in the experimental watershed.

Soil pCO_2 is controlled by the balance of production and consumption, where each process is regulated by environmental factors. However, understanding the controls on variation in soil pCO_2 is difficult due to the many variables that affect concentrations (Fig. 1), ranging from global atmospheric CO_2 concentrations, to landscape scale heterogeneities in bedrock, soil, ecosystems, and microclimate, to small scale variation in biology and the physical properties of soils. Biological influences on soil CO_2 include the distribution of leaf litter input, which provides a heterogeneous input to the C pool, as well as the subsurface distribution of plant roots and microorganisms that produce soil CO_2 through respiration (Tang and Baldocchi, 2005; Oh et al., 2005). Physical parameters such as soil temperature, moisture, pore space, and texture also influence soil CO_2 dynamics by regulating biological activity and diffusion rates (Kaye and Hart, 1998; Rayment and Jarvis, 2000; Law et al., 2001; Risk et al., 2002). In the literature, soil CO_2 dynamics are often modeled as a function of the soil temperature and moisture conditions (Cerling, 1984; Hamada and Tanaka, 2001; Tang et al., 2003, 2005; Sullivan et al., 2008) because these factors generally correlate well with biological activity and diffusivity of gases in soils. These environmental factors vary within watersheds (e.g., soil moisture and texture) and across seasons (e.g., soil temperature and moisture), leading to expected variations in soil pCO_2 across space and time. However, such variations have rarely been tested as most measurements and models of pCO_2 do not explicitly include the effects of topographic position.

While previous work has extensively examined seasonal (Solomon and Cerling, 1987; Burton and Beauchamp, 1994; Schulz et al., 2011; Ross et al., 2012), diurnal (Tang et al., 2003, 2005), geographic (Schulz et al., 2011), climatic (Oh and Richter, 2004), depth (Fisher et al., 1985; Benstead and Lloyd, 1996; Fierer et al., 2005), and vegetative (Buyanovsky and Wagner, 1983; Kaye and Hart, 1998) controls on CO_2 concentrations and fluxes, to our knowledge topographic controls on pCO_2 have been characterized at only two locations. In northeastern Spain, the variability in soil pCO_2 between two topographic positions within a single small catchment was as large as differences observed in two different mountain ranges (Piñol et al., 1995). In the northern Rocky Mountains, catchment-scale soil CO_2 dynamics were significantly influenced by landscape position; specifically, pCO_2 was highest in riparian zones due to higher soil moisture near the stream valley (Pacific et al., 2008; Riveros-Iregui et al., 2011). The timing of peak soil pCO_2 in the watershed also differed between landscape positions because of variability in the onset of snowmelt (Pacific et al., 2008). These studies suggest that topography may be a strong predictor of soil pCO_2, especially through its effect on soil moisture, which can act as a diffusion barrier.

While these studies compared ridge top versus valley floor topographic positions, the SSHCZO catchment has other topographic characteristics such as slope aspect and shape that may add complexity to spatial patterns in soil pCO_2. For example, the north and south sides of the watershed differ in their soil moisture content (Lin, 2006; Lin et al., 2006). Furthermore, on both sides of the catchment, the hillslopes experience either non-convergent, downslope flow (planar hillslopes) or convergent flow (swales). The swales, which comprise 23% of the watershed area (Andrews et al., 2011), are substantially wetter than the planar slopes (Lin, 2006; Lin et al., 2006).

Given the complex terrain and extensive soil moisture and temperature monitoring at the SSHCZO, it is an ideal location to examine how topography affects soil pCO_2. In this paper, we describe the depth distribution of soil pCO_2 across catenas within the SSHCZO watershed to determine whether topography may be a valuable parameter to include in analyses of soil pCO_2 and its relationship to weathering. We monitored soil pCO_2 on planar slopes, swale depressions, ridge tops, and valley floors with differing aspect, and throughout this paper, we refer to combinations of aspect, catena location (ridge top, mid-slope, and valley floor), and hillslope shape (swale versus planar) as "topographic positions." Our pCO_2 samples were collected at multiple depths to just above bedrock (B/C or C horizon; up to 2.4 m deep). We investigated these observations to ask: does the soil pCO_2 distribution vary predictably with topographic position in the SSHCZO? Answering this question will lead to more accurate models of soil CO_2 dynamics than those based on soil temperature and moisture alone as well as aid in estimating variation in weathering rates across forested landscapes.

2. Study site

Soil CO_2 samples were collected in a temperate, deciduous forest at the SSHCZO (Fig. 2A), a site established in central Pennsylvania to study the inter-relationships between hydrology, geomorphology, pedology, geochemistry, and ecology. The V-shaped catchment is 7.9 ha with a valley and an ephemeral stream that roughly align east-west. The watershed has an annual temperature of ~10 °C, but varies between −25° and 41 °C. The annual precipitation is ~1.00 m, with the highest rainfall months occurring in the early spring and fall. From 2008 to 2010, soil pCO_2 and microclimate were monitored along two south (north-facing) hillslopes. Three sites were located on a planar hillslope transect: south planar ridge top (SPRT), south planar mid-slope (SPMS), and south planar valley floor (SPVF), and the other three sites were along an adjacent swale transect: south swale ridge top (SSRT), south swale mid-slope (SSMS), and south swale valley floor (SSVF; see Fig. 2A). Additional monitoring of the mid-slope sites was conducted in 2013, and included sampling at SPMS and SSMS as well as sites on the north (south-facing) side of the catchment: north planar mid-slope (NPMS) and north swale mid-slope (NSMS; Fig. 2A).

The planar and swale hillslopes are convex-upward near the ridge and concave-upward near the valley floor. The planar hillslopes are defined as planar because they do not experience convergent flow of water and sediments; rather the flow is strictly vertical (one-dimensional) or directly downslope (two-dimensional). The swales, on the other hand, experience vertical, downslope, and convergent (three-dimensional) flow of water and

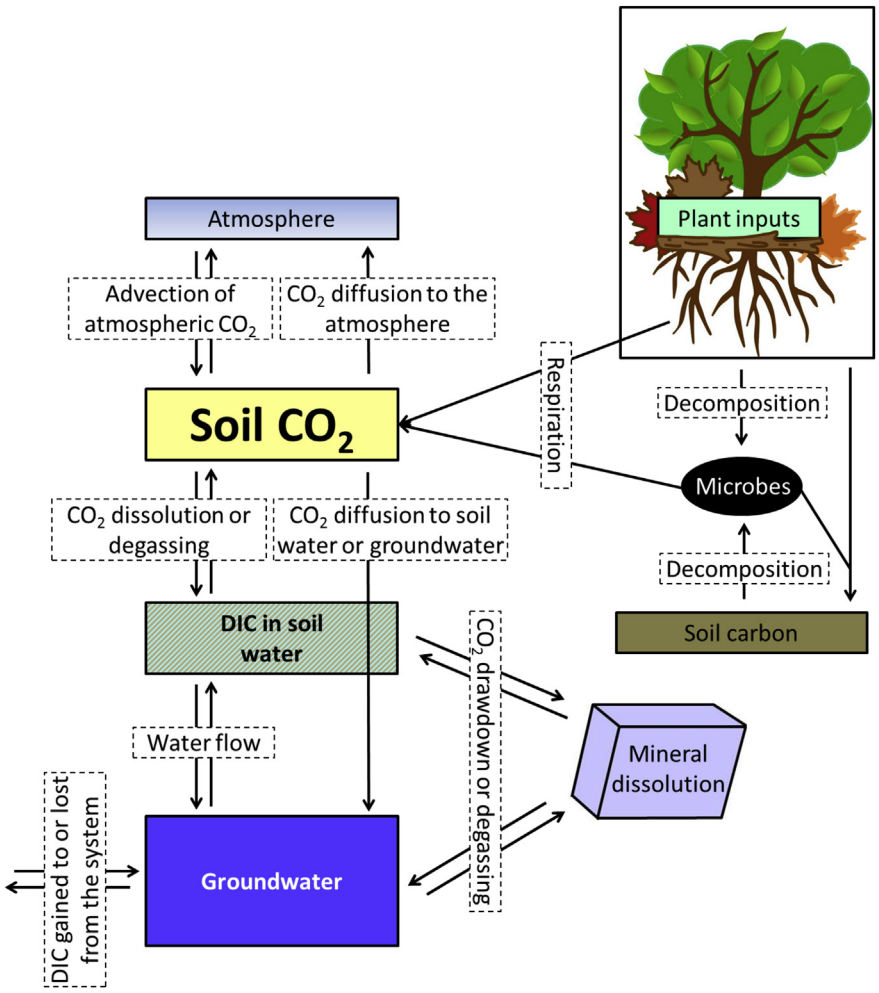

Fig. 1. Soil atmosphere pCO_2 reflects the balance of i) production of CO_2 by belowground cellular respiration, ii) diffusion of CO_2 out of the soil upward to the atmosphere or downward to soil water or groundwater, iii) CO_2 drawdown from or CO_2 degassing to porefluids during mineral dissolution (this process depends on what mineral(s) dissolve), iv) advection of dissolved inorganic C (DIC)-containing fluid into or out of the system, and v) advection of atmospheric CO_2 into air-filled soil pore spaces.

sediments. The south swale hillslope is unique in that the soil is anomalously thick at the mid-slope (e.g., 1.6 m at SSMS compared to 0.9 m at SSVF; Fig. 2B). Furthermore, there is a bend in the south swale at the mid-slope that can be observed in Fig. 2A.

The entire catchment is underlain by Silurian Rose Hill Formation shale (Berg et al., 1980). Compositionally, the shale consists of quartz, illite, chlorite, vermiculitized chlorite, Fe oxides, minor feldspar, and, at depth, variable amounts of Fe–Mn–Ca carbonates (Jin et al., 2010). Soil thickness varies through the catchment from <0.25 m on the ridge tops to >2 m in the valley and swale depressions (Lin, 2006). Prior work has reported soil geochemistry and mineralogy for catenas along the planar hillslope (Jin et al., 2010; Ma et al., 2011a) and a swale hillslope (Jin and Brantley, 2011). Briefly, the soils contain no carbonate, and chlorite and illite are weathering to vermiculite, hydroxyl-interlayer vermiculite, Fe oxides, and minor amounts of kaolinite. Andrews et al. (2011) reported the distribution of soil organic C (representing 41% of the soil organic matter (SOM) content) in the catchment: the swales have 22% more soil organic C storage in the solum (down to ≤ 1.1 m) compared to the planar slopes (see Table S1 in the Supplementary material). At the swale valley floor, dissolved organic C (DOC) concentrations within the top 0.4 m were 40% higher than for the equivalent planar slope position (Andrews, 2011; Andrews et al., 2011; Table S1).

There are five distinct soil series in the watershed (Fig. 2A) identified by Lin (2006) and Lin et al. (2006), which include the (1) Weikert (loamy-skeletal, mixed, active, mesic Lithic Dystrudepts), which dominates the catchment (area = 78.7%) and occurs on hilltops or convex hillslopes with a depth to fractured bedrock of <0.5 m, (2) Berks (loamy-skeletal, mixed, active, mesic Typic Dystrudepts), which is largely distributed along transitional slope zones between the Weikert and the deeper Rushtown with depths of 0.5–1.0 m to bedrock (area = 9.8%), (3) Rushtown (loamy-skeletal, over fragmental, mixed, mesic Typic Dystrudepts), which dominates the center of swale depressions as well as a large area in the back of the catchment and consists of deeper soils (>1.0 m; area = 6.3%), (4) Ernest (fine-loamy, mixed, superactive, mesic Aquic Fragiudults), a deeper soil (>1.0 m) that dominates the valley floor and exhibits many redox features (area = 4.9%), and (5) Blairton (fine-loamy, mixed, active, mesic Aquic Hapludults), another deeper soil (>1 m) that makes up a small portion of the valley floor (area <0.3%). The pCO_2 monitoring sites are located on the Weikert (SPRT, SPMS, SSRT, and NPMS), Rushtown (SSMS, SSVF, and NSMS), and Ernest (SPVF) soil series. Soil horizons in Tables S1 and S2 are estimated based on the findings of Lin (2006) and Thomas et al. (2013). These findings agree with in situ observations of the south planar transect by Jin et al. (2010). An Oe-horizon covers the upper ≤0.05 m of the entire catchment. Other

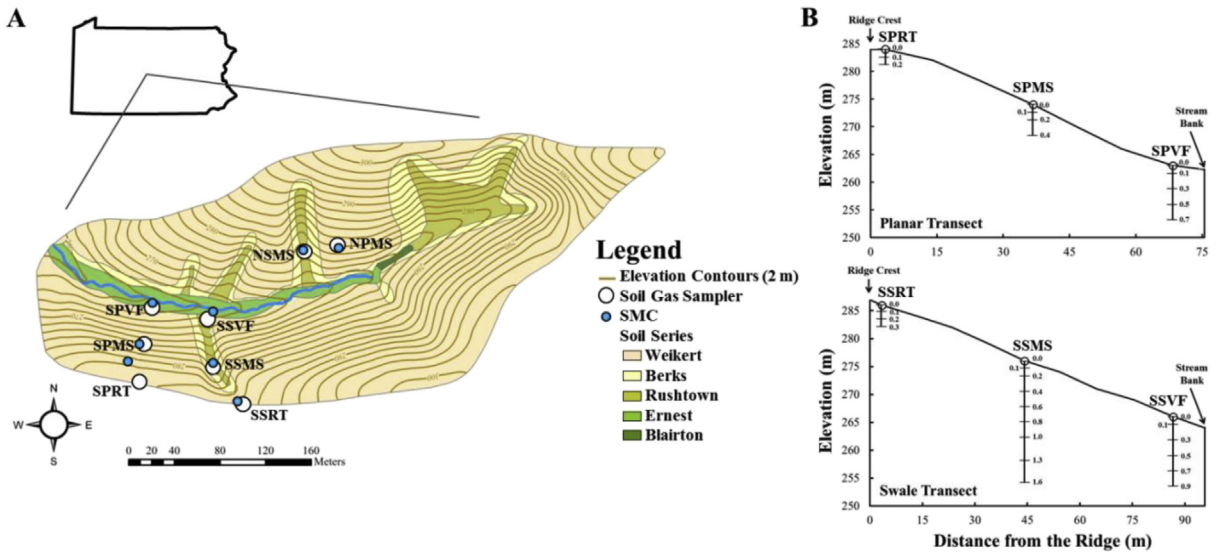

Fig. 2. (A) Sampling locations within the SSHCZO catchment. Colors indicate soil types based on field surveys by Lin et al. (2006). The first-order ephemeral stream (blue), soil CO_2 gas sampling locations (large, open circles), and soil moisture measurement sites (small, blue circles) are shown. Soil CO_2 gas samplers are located along the south planar (i.e., SPRT, SPMS, and SPVF), south swale (SSRT, SSMS, and SSVF), north planar (NPMS), and north swale (NSMS) hillslopes. The south slope sampling locations are all within a few meters of sites discussed in previous papers (Jin et al., 2010; Jin and Brantley, 2011; Ma et al., 2011a). (B) A schematic of elevation versus the distance from the ridge with the gas sampler locations noted for the south planar and swale transects. The nested soil gas sampler depths are not to scale. (For interpretation of the references to color in this figure legend, the reader is referred to the web version of this article.)

physiochemical properties for the sites can be found in Tables S1 and S2 in the Supplementary material.

The majority of the SSHCZO watershed is covered by deciduous trees that consist of oaks that dominate throughout the watershed, maples that occur on northern slopes, and hickories found on northern slopes and southern ridge top (Naithani et al., 2013). Conifers are less abundant than deciduous species, but are still common and include Eastern hemlocks, which are located predominantly in the valleys, and pines, which are generally located on the ridge tops (Naithani et al., 2013). The tree species density and distribution were mapped by Eissenstat et al. (2013).

3. Methods

3.1. Soil CO_2 concentration

To measure soil pCO_2 levels in the SSHCZO watershed, gas samplers (de Jong and Schappert, 1972) were installed following a modified U.S. Geological Survey (USGS) protocol (Schulz, 2006) at the south planar transect (August 2008), south swale transect (July 2009), and north mid-slopes (August 2013). Specifically, vertical soil gas samplers were constructed of 3.18 mm stainless steel tubing (inner diameter = 2.16 mm) and cut to the desired sampling depth plus an additional 0.1–0.3 m (for surface access). Stainless steel mesh (0.2 mm openings) was cut to 0.05 by 0.08 m, wrapped around one end of the stainless steel tubing, secured with epoxy, and crimped once the epoxy dried to prevent the sampler from clogging with soil. Brass compression fittings and Swagelok end caps were installed on the other end of the tubing along with a three-way connector. Holes were hand-augered at the sampling sites to the desired depth and the recovered soils were sieved using a 2 mm sieve. A gas sampler was placed at the bottom of the auger hole, and 0.05 m of sieved coarse fragments (>2 mm) were added to ensure good air circulation around the sampler. Instead of using bentonite (i.e., Schulz, 2006), which could "contaminate" ongoing silicate weathering studies at the SSHCZO, we added 0.05 m of the sieved soil (<2 mm) above the coarse fragments to discourage vertical air movement. The hole was then back-filled with the remaining soil. If more than one sampler was placed in the same auger hole, the process was repeated; however, for samplers placed higher in the soil profile an additional 0.05 m layer of sieved soil, covered by another 0.05 m of coarse fragments, was added below the desired sampler depth.

Soil gas samplers were generally placed at depth increments of 0.2 m until reaching the layer of refusal by hand augering, just above the impenetrable bedrock. However, in thin soils and near the soil surface, smaller intervals (0.1 m) were used to measure pCO_2 variation at or near soil horizons (see Tables S1 and S2; Fig. 2B) to provide additional insight into the influence of soil horizonation on CO_2 gas processes. The representative soil horizons were estimated based on in situ observations and each gas sampler nest's location relative to surveyed soil series and soil-bedrock interface maps (Lin, 2006; Tables S1 and S2). The same depth intervals were used at gas sampling sites with similar hillslope locations. For example, the depth intervals for the mid-slope sites are the same down to 0.4 m, which is the depth of refusal at SPMS; however, SSMS, NPMS, and NSMS have additional sampling intervals due to deeper soil.

Soil gas samples were collected from the south planar transect from August 2008 to August 2010 and swale transect from July 2009 to August 2010. Samples were collected 24 times during the growing season (April to September) and 14 times during the non-growing season (October to December; see Fig. S1 in the Supplementary material). Fewer samples were collected during the non-growing season because soils were often frozen and respiration rates were low. An additional suite of soil gas samples was collected on seven occasions from August 2013 to December 2013 at the mid-slope positions on both the north and south slopes (Fig. S2) to determine how aspect affects soil pCO_2. The 2008–2010 and 2013 soil CO_2 gas samples were generally collected weekly, and to be consistent, the sampling occurred between 10:00 and 15:00.

During site visits, soil CO_2 samples were obtained by connecting a 60 mL gas-tight syringe to the sampler's three-way port. To assure gas samples were representative of the depth of interest, the

samplers were purged of air prior to sample collection. Gas samples were either stored in the syringe if they were to be analyzed within 48 h or were immediately transferred from the syringe with a needle to pre-evacuated 15-mL Labco® glass vials for longer storage before laboratory processing. The Labco® vials were overpressured with soil gas to prevent contamination during storage. Atmospheric pCO_2 samples were collected at a height <0.02 m above surface leaf litter during every gas sampling excursion using syringes or Labco® vials for storage.

Sample CO_2 concentrations were analyzed in the laboratory using an infrared gas analyzer (IRGA; LI-7000, LI-COR Inc., Lincoln, NE). The sample injection volumes ranged from 1 to 5 mL and the instrument flow rate was 0.4 L min^{-1}; instrument accuracy is 1% of the sample value. Sample runs were calibrated with six CO_2 standards (Gas and Technology Services Inc., Santa Maria, CA) ranging from 500 to 10,300 ppmv. Atmospheric pressure (P in Pa) was calculated from the hillslope elevation above sea level (h_a in m) using a relationship developed by Kutz (2006):

$$P = 101325\left(1 - 2.25577 \times 10^{-5} h_a\right)^{5.25588} \quad (4)$$

Using Eq. (4), we converted IRGA data from the lab to pCO_2 in the field using the ideal gas law along with field soil temperature. The influence of weather on atmospheric pressure is minor compared to differences in elevation, so we used only sampling site elevations obtained from digital elevation model (DEM) data for the watershed (SSHCZO, 2013) to calculate pCO_2. Sensitivity analyses of Fick's law of diffusion to soil porosity, moisture, and temperature were conducted using a modified CO_2 flux calculation from Tang et al. (2005).

3.2. Soil microclimate

In addition to soil pCO_2 measurements, we also monitored the soil microclimate (i.e., soil moisture and temperature) at the study sites. Volumetric soil moisture content was measured approximately weekly using time domain reflectometry (TDR) at multiple depths (Figs. S3 and S4) near the nested gas samplers. In particular, a TRIME-T3 tube access probe and a TRIME-FM3 mobile moisture meter (IMKO, Ettlingen, Germany) were used to measure soil moisture; see Lin (2006) and Lin et al. (2006) for details. Where soil moisture depths did not match gas sampler depths, the soil moisture was estimated using a weighted mean of the two nearest depth increments. Likewise, it was not always possible to collect soil moisture data at all of the sites on the same date. However, linear regressions between sites were used to approximate soil moisture at sites lacking data when soil moisture was measured at other locations.

Prior to 2013, soil temperature data were measured with an ST09 digital thermometer (Supco, Allenwood, NJ) at a depth of 0.07 m. In 2013, soil temperatures were recorded at various depths with automated 5TE temperature sensors (Decagon Devices, Inc., Pullman, WA). Like the soil moisture sampling locations, when gas sampler depths did not match the temperature measurement depths, a weighted mean was used to approximate the soil temperature for the depth of interest. The soil microclimate data at SPRT, SPMS, SPVF, SSRT, SSMS, SSVF, NPMS, and NSMS (Fig. 2A) correspond with sites 10, 8, 6, 14, 12, 11, 60, and 51/55, respectively, previously discussed by Lin (2006) and Andrews (2011).

3.3. Statistical analyses

A repeated-measures analysis of covariance (RM-ANCOVA) test was used to examine the effects different topographic positions (planar or swale slopes and ridges, slopes, or valleys), soil depths, soil moisture content, soil temperatures, seasons (i.e., time), and their interactions had on soil pCO_2 (Table 1). The RM-ANCOVA tests the equality of means and is used when the dependent variable is measured under a number of different conditions that include continuous variables (Delwiche and Slaughter, 2003). The Type III test was performed using a mixed linear model, the *proc mixed* procedure, in SAS (version 9.4, SAS Institute, Cary, NC) with a split-plot approach and randomized block design after Andrews et al. (2011). In detail, each topographic position has multiple soil depths; therefore, the topographic position is considered as the main plot factor and the soil depth is treated as the subplot factor that is nested within the topographic position. The code also includes a repeated-measures statement where variation in pCO_2 was modeled through time. Seasonality was used as the temporal variable.

The *proc mixed* procedure was also used to examine the effects of various C sources in the soil on pCO_2. The C sources include measurements made by Andrews (2011) and Andrews et al. (2011) of SOM, total soil C, and porewater DOC within ~1 m of our monitoring sites; details of sample collection and analysis can be found within these references. The mixed linear model effects include topographic position, soil depth, SOM, total soil C, and porewater DOC. Because the effects (i.e., SOM, total soil C, and porewater DOC) have a non-normal distribution we modeled the data using both maximum likelihood estimation (ML) and minimum variance quadratic unbiased estimation (MIVQUE0) methods, where the latter is better suited for non-normal estimators (Rao, 1971). The Akaike's Information Criteria (AIC; Akaike, 1974) estimate shows that the *proc mixed* model using the MIVQUE0 (AIC = 243.7) is a better fit over the ML (AIC = 403.6) method, where smaller AIC is a better fit. No additional effects or interactions were included in the model because of the limited number of data ($n = 23$). The Type III test for fixed effects shows the significance of each effect in the overall model statement (Table 2).

Additionally, t-tests conducted in SAS were used to determine the significance of the average pCO_2 values for different topographic positions (significance of $p < 0.05$). Measurements from the same sampling day were paired and repeated measurements over time constituted the replication of the paired comparison.

4. Results

4.1. Soil microclimate

4.1.1. Soil temperature

Soil temperatures (at 0.07 m) ranged from 9.7 to 20.6 °C during the 2008–2010 study period. The average soil temperatures (Table S1) and standard deviations were not significantly different between the sampling locations along the south slope sites and

Table 1
Type III test showing significance of partial effects with all other effects in the RM-ANCOVA mixed linear model.

Effect	F Value	$P_r > F$
Topographic position	2.85	0.0148
Depth	9.78	0.0018
Moisture content	29.72	<0.0001
Temperature	0.42	0.5181
Topographic position*Depth	23.19	<0.0001
Topographic position*Moisture content	5.57	<0.0001
Topographic position*Temperature	2.08	0.0656
Topographic position*Seasonality	2.66	0.0006
Depth*Moisture content	1.13	0.2887
Depth*Temperature	0.40	0.5271
Depth*Seasonality	11.25	<0.0001

Table 2
Type III test of fixed effects using a mixed linear model.

Effect	F Value	$P_r > F$
Topographic position	5.34	0.0070
Depth	43.14	<0.0001
SOM	0.02	0.8900
Total soil C	2.84	0.1156
Porewater DOC	0.79	0.3915

were within 0.3 and 0.4 °C of each other, respectively. In 2013, soil temperatures ranged from 4.3 to 22.5 °C, and temperature variations were the highest at the soil surface and decreased with depth (Table S2). On the south slope, the average shallow (<0.4 m) soil temperatures were similar between SPMS and SSMS (i.e., 15.2 versus 15.1 °C; $p = 0.60$). Below 0.4 m, the average temperature in the deeper SSMS profile was 10.3 °C, close to the average air temperature at SSHCZO. On the north slope, soil temperatures above 0.4 m were >1 °C higher than the south slope and varied significantly between the planar and swale hillslope profiles (NPMS = 16.3 °C and NSMS = 17.9 °C; $p << 0.01$). Deeper in the profiles, the average temperatures were 15.7 °C and 16.1 °C for NPMS and NSMS, respectively; significantly higher than the temperatures observed below 0.4 m on the south slope ($p < 0.01$). Thus, aspect (south versus north) has a significant effect on the soil temperature at depth >0.4 m.

4.1.2. Soil moisture

From 2008 to 2010, the soil moisture at the ridge top (SPRT and SSRT) ranged from 0.046 to 0.247 $m^3\ m^{-3}$ (Fig. 3, Fig. S3), and was not significantly different ($p = 0.22$) at equivalent depth intervals. Valley floor soils ranged from 0.132 to 0.555 $m^3\ m^{-3}$ (Fig. 3, Fig. S3), with higher and more variable soil moisture observed at SPVF compared to SSVF ($p << 0.01$, Table S1). The valley floor positions near the stream had significantly ($p << 0.01$) wetter soils than the ridge top hillslope positions (Figs. 3 and 4). The mid-slope sites (SPMS and SSMS) had the most disparate soil moisture values (0.051–0.385 $m^3\ m^{-3}$; Fig. 3, Fig. S3) between equivalent depths ($p << 0.01$; Table S1), with the wettest conditions occurring at SSMS. Indeed, SPMS had similar moisture conditions compared to the ridge tops while SSMS was similar to the valley floor positions (Table S1; Figs. 3 and 4).

In 2013, we tested the influence of aspect on soil moisture at equivalent depths. Over the study period, soil moisture ranged from 0.025 to 0.405 $m^3\ m^{-3}$ for all the mid-slope sites (Fig. S4). As observed in the 2008–2010 data, there was a significant difference in the soil moisture between the swale and planar mid-slopes on both sides of the catchment. Specifically, NPMS was drier than NSMS ($p = 0.03$), and likewise SPMS was drier than SSMS ($p << 0.01$; Table S2; Fig. S4). SPMS was drier than NPMS ($p << 0.01$), while NSMS was drier than SSMS ($p < 0.01$; Table S2; Fig. S4).

Generally, soil moisture increased with depth; however, with the exception of SSRT, this increase was not always uniform (Tables S1 and S2; Figs. 3 and 4, Figs. S3 and S4). In particular, zones of high soil moisture generally occurred along soil horizon interfaces, and both shallow (i.e., SPRT, SPMS, and NPMS) and deep (i.e., SPVF, SSMS, SSVF, and NSMS) soils displayed these anomalies. In the shallow profiles, localized soil moisture maxima were observed along the A–B horizon transition (i.e., 0.1–0.2 m), whereas in the deeper profiles, the localized maxima occurred around the B–C interface (i.e., ~0.6 m).

The south slope (2008–2010) had similar seasonal patterns in soil moisture (Fig. 3, Fig. S3). Specifically, for all the south slope sites, soil moisture was high beginning in the early spring and decreased to its minimum value in the late summer. The lowest soil moisture values occurred in August in the shallower, drier profiles and September in the deeper, wetter profiles. In the fall, soil moisture increased again, especially in the deeper soil profiles, reaching its highest values in November and December (Fig. 3, Fig. S3). Indeed, at times during the winter we were unable to collect gas samples from SPVF and SSMS because the soils were completely saturated. In 2013, the wettest soil conditions occurred earlier in the summer (i.e., July; Fig. S4) due to heavy rainfall. However, soil moisture reached minimum values in September and began to increase in October, similar to the 2008–2010 observations.

4.2. Soil pCO_2

Soil pCO_2 in the catchment varied from near atmospheric concentrations to more than 35,000 ppmv, with the highest pCO_2 occurring in the deepest, wettest soils: SPVF (0.7 m), SSVF (0.9 m), SSMS (1.6 m), and NSMS (2.4 m; Tables S1 and S2; Figs. 5 and 6). On the south slope, pCO_2 was low at the ridges and high in the valleys (Fig. 4). Differences in pCO_2 between the planar and swale slopes were smallest at the ridge tops ($p = 0.14$) and largest at the mid-slope positions ($p << 0.01$; Tables S1 and S2; Figs. 5 and 6). For equivalent depth intervals at the mid-slopes, pCO_2 was higher and more variable (i.e., the standard deviation) at SSMS than SPMS. Indeed, the pCO_2 level and variability at SPMS was comparable with the ridge tops (Table S1). For example, the average pCO_2 for SPMS at 0.4 m was almost 6,000 ppmv less than SSMS at 0.4 m (Table S1). With regard to slope aspect, pCO_2 differs significantly ($p = 0.04$) in the swales, where SSMS has higher pCO_2 for the same depth when compared to NSMS. In contrast, the pCO_2 in the planar mid-slopes do not vary significantly with aspect (i.e., SPMS versus NPMS; $p = 0.19$).

Seasonal changes in soil pCO_2 were similar across the sites, though the largest fluctuations were observed in deep soils (Figs. 5 and 6). During the 2008–2010 sampling period (i.e., south slope), pCO_2 rose in the early spring, peaked in June, and subsequently declined in July and August. After August, pCO_2 increased again, especially deep in the soil profile; however, the fall pCO_2 peak was not as large as the June peak (Fig. 5). The peak pCO_2 observed in the 2013 data (i.e., north and south mid-slopes) occurred in August, and declined in the fall and winter (Fig. 6). Soil pCO_2 variability between sites increased during the spring and fall pCO_2 peaks (Figs. 5 and 6, Figs. S1 and S2), with the largest changes in the deeper soils. For example, pCO_2 differences were large between swale mid-slopes at equivalent depths during the summer, but these differences decreased during the winter (Fig. 6). In contrast, at the planar mid-slopes, pCO_2 differences between the north and south slopes were small in both the summer and winter. Seasonality can influence the soil microclimate, and we observed a positive correlation between soil moisture and pCO_2, but no correlation between soil temperature and pCO_2 (Figs. S5 and S6).

Soil pCO_2 generally increased with soil profile depth (Figs. 5 and 6, Figs. S1 and S2) and was correlated negatively with porosity and positively with bulk density for all the profiles (Figs. S5 and S6). The pCO_2 variability also increased with depth (i.e., pCO_2 standard deviations were positively correlated with average pCO_2; Tables S1 and S2). Occasionally, SPRT, SSMS, SSVF, and NSMS exhibited localized, high pCO_2 values (Figs. 5 and 6; see asterisks). These anomalies generally occurred during the early spring and summer at depths between 0.5 and 1.0 m (i.e., B and C horizons).

The RM-ANCOVA output supports the correlations observed between topographic position and soil pCO_2 (Table 1). The partial effects of topographic position, depth, and soil moisture were significant terms in the mixed linear model. There were also many

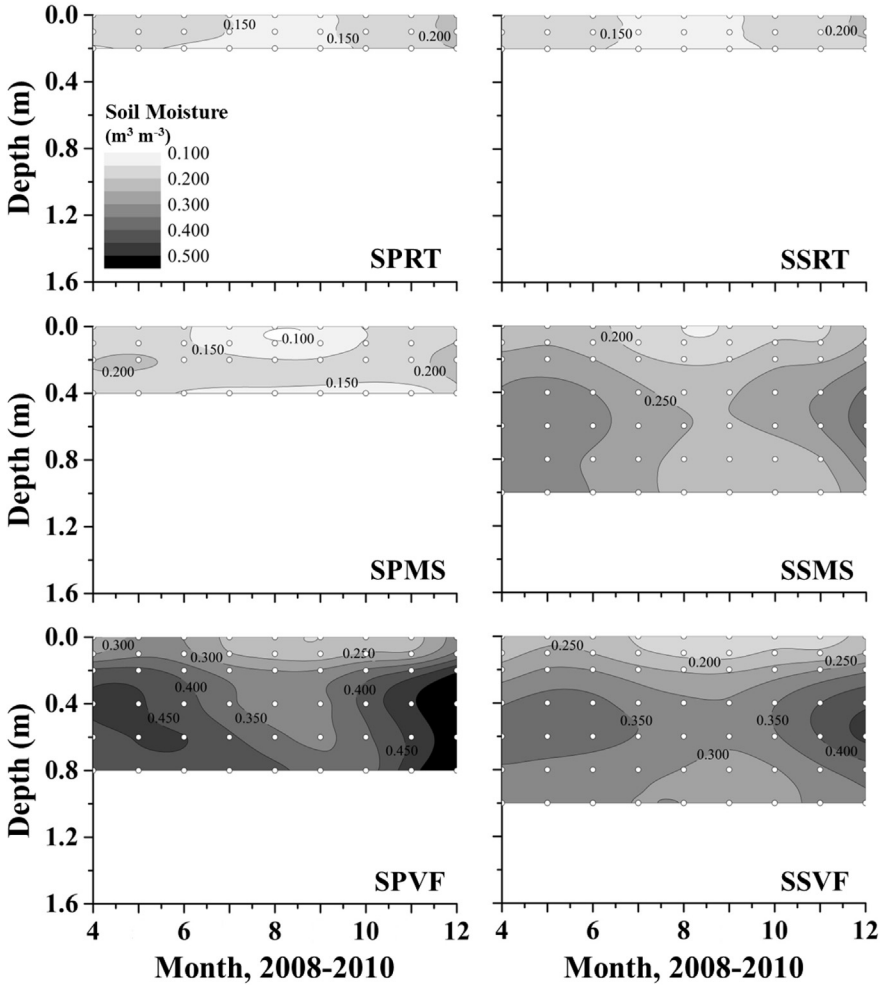

Fig. 3. Contour plots of average monthly volumetric soil moisture ($m^3\ m^{-3}$) as a function of soil depth (m) and time (month, averaged for 2008–2010) on the south slope. Sampling was not possible from January to March as the soil was frozen during this time. Small circles indicate sampling depth; note that they do not always match the gas sampler depths (i.e., all are in 0.1, 0.2, 0.4, 0.6, 0.8, and 1.0 m increments). Because surface (i.e., 0.0 m) soil moisture data were not available, we assumed that soil moisture at 0.0 m was approximated by the soil moisture at 0.1 m to interpolate the contour plots.

significant interactions. The effect of topographic position depended on depth (Topographic position*Depth: $p < 0.0001$); in other words, topographic position effects were most pronounced deeper in the soil profiles. Similarly, the effect of topographic position (Topographic position*Seasonality: $p = 0.0006$) and depth (Depth*Seasonality: $p < 0.0001$) depended on seasonality because topographic position and depth effects on pCO_2 were most pronounced early in the growing season. Interestingly, while the effect of topographic position depended on soil moisture (Topographic position*Moisture content: $p < 0.0001$), the effect of depth did not (Depth*Moisture content: $p = 0.289$). This is because the effect of topographic position was most pronounced at higher soil moisture values, while the basic trend of increasing pCO_2 with depth was similar in wet and dry soils. Temperature was never a significant direct or interactive term in the model. In our mixed linear model to assess the effects of various C sources on soil pCO_2 (Table 2), topographic position and depth were the only significant effects ($p = 0.0070$ and $p < 0.0001$, respectively) on soil pCO_2; SOM, total soil C, and porewater DOC were not significant ($p > 0.05$).

5. Discussion

Data from SSHCZO clearly show that topographic position is a strong predictor of soil pCO_2. In detail, location along the catenas was the strongest predictor of soil depth, texture, porosity, and moisture, all important controls on soil pCO_2 content. The almost 7-fold variation in pCO_2 we observe across topographic positions could indeed impact weathering through enhanced porewater acidity. Here, we interpret this variation in relation to mechanisms that lead to topographic variation in pCO_2: landscape-scale variation in soil water and its effects on biologically produced CO_2 (i.e., soil respiration) as well as the upward diffusion of that CO_2.

5.1. Relationship of soil pCO_2 to landscape controlled microclimate

Our temperate, forested catchment has similar vegetation and geology throughout, and thus the distribution of soil moisture is conditioned by the joint effect of topography and soil characteristics. Therefore, a combination of terrain attributes and soil moisture patterns provides a good interpretation of observed soil pCO_2 distribution. Intermediate soil moisture values generally promote higher soil pCO_2 (Davidson et al., 2000; Pacific et al., 2008), and optimal soil respiration occurs at soil moisture levels of ~25% (Tang and Baldocchi, 2005). Furthermore, high soil moisture acts as a diffusion barrier, so even if moisture levels are not ideal for soil respiration, any CO_2 produced by biological activity is trapped in the soil. Thus, in locations where soil moisture values were low (i.e., the ridge tops and planar mid-slopes), pCO_2 was also low, while in

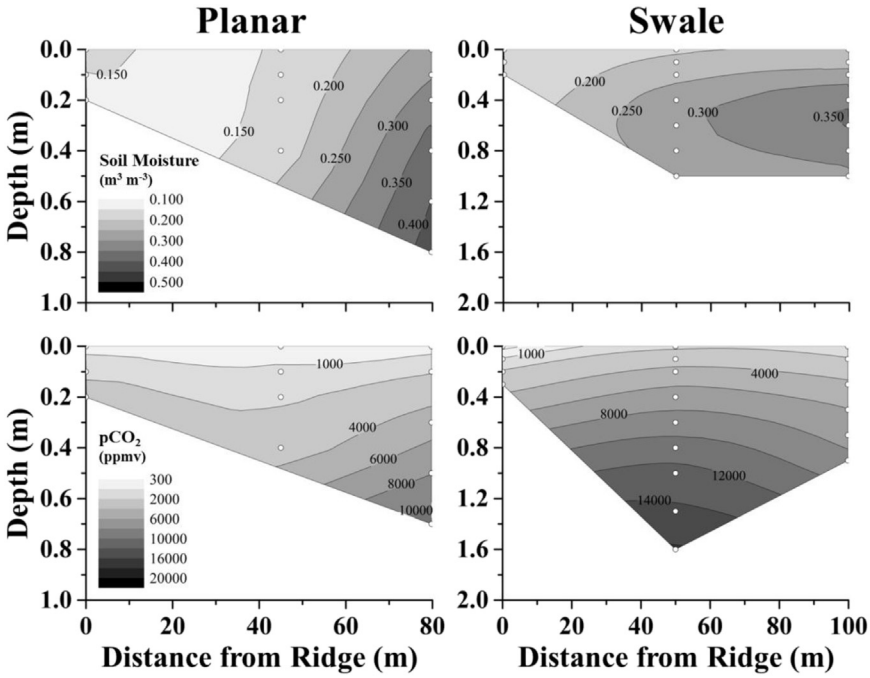

Fig. 4. Contour plots of soil moisture ($m^3\ m^{-3}$; top panels) and pCO_2 (ppmv; bottom panels) for 2008–2010 as a function of distance from the southern ridge top and depth along a planar slope (left panels) or a swale slope (right panel). Small circles indicate sampling depth locations. Note the differences in the y-axis (depth) scales.

locations of high soil moisture there was also high pCO_2.

Sensitivity analyses of Fick's law of diffusion to soil porosity, moisture, and temperature demonstrate the relative importance of various soil parameters on soil CO_2 contents (Fig. S7). We calculated the response of pCO_2 and CO_2 flux to variations in these parameters and found that porosity and moisture levels are significant controls on soil pCO_2. This corresponds to the strong negative correlation between porosity and pCO_2 and strong positive correlation bulk density and pCO_2 (Figs. S5 and S6). These relationships are consistent with soil physical properties and gas diffusivity (Møldrup et al., 2003; Šimůnek and Suarez, 1993). Depth is an important control on the soil porosity, and increasing soil depth generally reduces porosity (Tables S1 and S2). Low porosity reduces CO_2 diffusion, allowing pCO_2 levels to increase in the deeper soils. Additionally, our sensitivity calculations show that soil moisture also strongly controls the pCO_2 (Fig. S7). This is in agreement with the correlation observed between soil moisture and pCO_2 at our sites (Figs. S5 and S6) and previous findings (Cerling, 1984; Hamada and Tanaka, 2001; Tang and Baldocchi, 2005; Sullivan et al., 2008). Importantly, both soil depth (and therefore soil porosity) and moisture content are dependent on topographic position. However, over the range of temperatures observed in this study, soil temperature does not play an important role in CO_2 flux (Fig. S7), which corresponds to the weak relationship between temperature and pCO_2 observed in Figs. S5 and S6.

5.2. Spatial variability within and between topographic positions

Geomorphologists have long known that swales concentrate the flow of water and sediments, which leads to thicker soil profiles. In turn, the vertical variability in soil properties (including depth) controls the subsurface hydrology and pCO_2. Thus, we hypothesize that globally swales are more effective short-term reservoirs for soil pCO_2 than planar and convex slopes. Given that the ridge top sites are more or less identical, except for the hillslope below them, our two sites expectedly show only rather small differences in depth to bedrock, soil moisture, and soil pCO_2. Like the ridge tops, the planar and swale valley floors are geomorphologically similar except for the slope above them. We found that the valley floor locations have higher soil moisture values and pCO_2 than the ridge tops, which is in agreement with the results of Pacific et al. (2008). This demonstrates that higher soil moisture levels at the valley floor act as a diffusive barrier to soil pCO_2 allowing it to accumulate in the soil, while the dry ridge top experiences higher CO_2 diffusion rates and therefore lower pCO_2. Nevertheless, the water table (or possibly a migrating wetting front) is closer to the land surface at SPVF than SSVF. Consequently, the two valley floor sites have similar soil moisture, and thus similar pCO_2, above 0.5 m, but below 0.5 m SPVF has higher soil moisture and pCO_2 values (Figs. 3 and 5). On several occasions during the spring wet season, water was drawn from the 0.5 and 0.7 m deep SPVF gas samplers indicating the water table had reached depths of 0.5 m, but water was never observed in SSVF gas samplers. The Mg concentrations and H/O isotopes in soil waters at SPVF observed by Jin et al. (2011) indicate that the water table rises to the depths of the gas samplers.

The mid-slope positions have the most disparate geomorphology, soil moisture, and soil pCO_2 of all the topographic positions along the south planar and swale transects. The higher and more variable pCO_2 at SSMS compared to SPMS is due to the greater soil depth and higher soil moisture content of the SSMS profile (Tables S1 and S2; Figs. 3–5). In detail, water only moves vertically in the unsaturated zone except when there is ponding at a permeability barrier. Without ponding, the rate of vertical water movement will be the same between the ridge top, mid-slope, and valley floor sites. However, if there are horizontal layers of contrasting permeability, as is the case at the SSHCZO (Lin, 2006; Jin et al., 2011), then ponding and subsequent down-hillslope flow will occur (i.e., movement of water along preferential flowpaths, known as interflow). The hillslope at SPMS is steep (47.5% slope; Table S1) and does not experience convergent (three-dimensional) flow of water. Therefore, the soil is well-drained leading to low soil moisture (Fig. 3, Fig. S1). In contrast, the land surface at SSMS is shallower (27.9% slope; Table S1), which limits drainage. In addition, convergent flow along the swale channelizes water into SSMS,

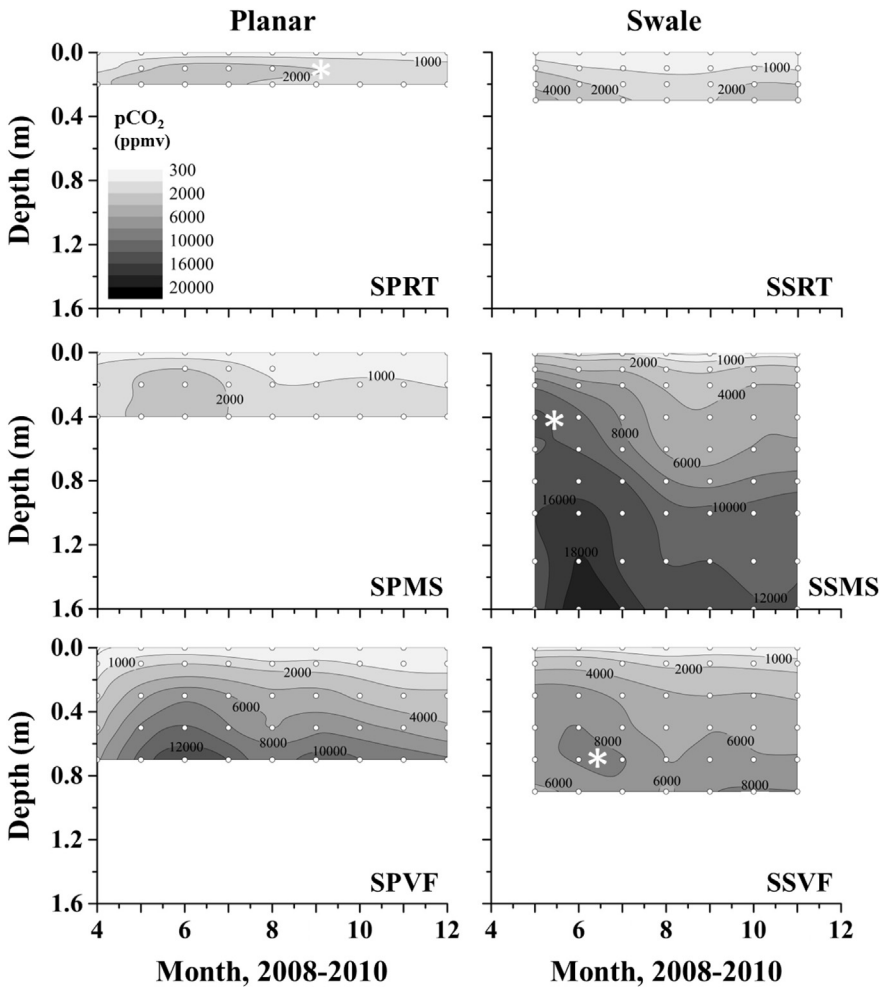

Fig. 5. Contour plots of average monthly soil pCO_2 (ppmv) as a function of soil depth (m) and time (month, averaged for 2008–2010) for soil gas monitoring sites on the south slope. Sampling was not possible from January to March as the soil was frozen during this time. Small circles indicate sampling depth and asterisks show areas with anomalously high pCO_2.

leading to higher and more variable soil moisture (Fig. 3, Fig. S1). Thus, SSMS maintains higher pCO_2 near the soil surface than SPMS because soil moisture acts as diffusive barrier.

Our results clearly show that topography controls soil depth, texture, porosity, and moisture, which govern diffusive loss of CO_2 from the soil to the atmosphere. In contrast, we found that parameters influencing the biological production of soil pCO_2 (Fig. 1), including SOM, total soil C, and porewater DOC, were not statistically significant effects on soil pCO_2 (Table 2). SOM, total soil C, and porewater DOC tended to be highest near the soil surface, where soil pCO_2 was lowest (Tables S1 and S2). This indicates that despite a higher potential for C to be respired to CO_2 near the soil surface, soil pCO_2 remains low here because production is outpaced by higher diffusion rates due to lower soil moisture and higher porosity. In other words, even though there may be more source C near the surface, there is nothing to trap the CO_2 in the soil profile. Thus, soil C storage is not predictive of soil pCO_2 patterns across the catchment. Collecting root density and respiration data from these topographic positions is an area of future research, which will provide additional details about differential CO_2 production.

5.2.1. Aspect

Aspect is an important topographic variable that likely enhanced pCO_2 differences in wet, swale mid-slopes (i.e., SSMS and NSMS), but was less important for the well-drained planar slopes (i.e., SPMS and NPMS). This difference between the swale mid-slopes cannot be attributed to depth, as NSMS is deeper than SSMS. Furthermore, soil C sources differences, including soil organic C and porewater DOC, do not explain the variability. In detail, Andrews (2011) and Andrews et al. (2011) observed that NSMS has higher soil organic C in the A horizon and $\leq$1.1 m solum (~3.0 g cm^{-2}) as well as higher porewater DOC (A horizon = ~4.0 g cm^{-2} and $\leq$1.1 m solum = 1.8 g cm^{-2}) than SSMS, confirming our findings that the relationship between soil C sources and pCO_2 is not statistically significant (Table 2). Thus, the pCO_2 differences between the two swale mid-slopes are likely due to the soil moisture differences (Table S2; Fig. S4). The north (south-facing) slope receives more solar radiation than the south (north-facing) slope. This factor likely leads to both higher vegetative coverage (Eissenstat et al., 2013) and higher evapotranspiration rates, and consequently, lower soil moisture in the north swale mid-slopes (Lin, 2006). The lower soil moisture in the northern swales allows higher CO_2 diffusion and thus lower soil pCO_2. At the planar mid-slopes, however, higher slopes lead to better draining of the soils, and consequently, differences in soil moisture, and thus pCO_2, due to aspect are not important at these sites.

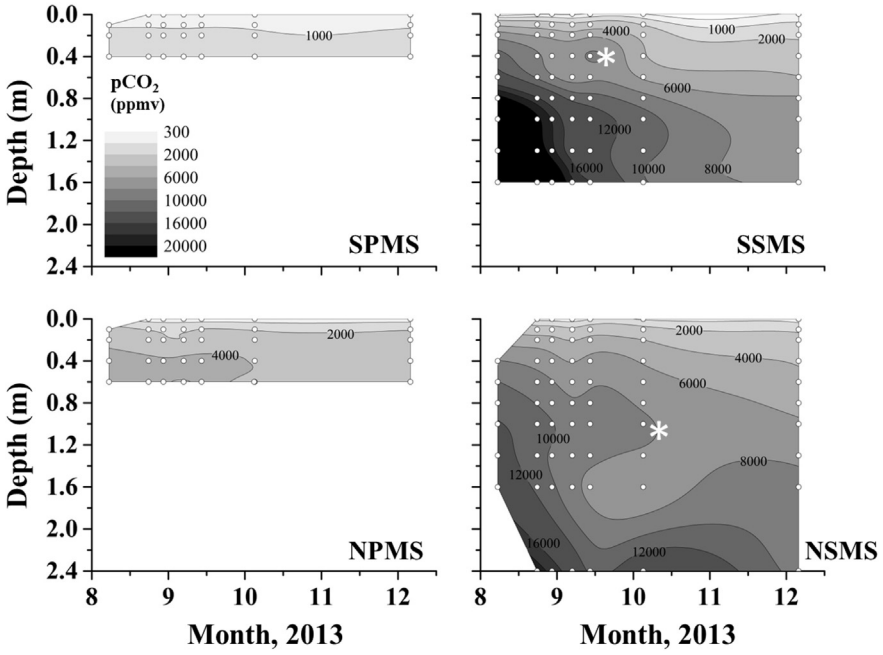

Fig. 6. Contour plots of soil pCO_2 (ppmv) as a function of soil depth (m) and time (month; individual sampling events for 2013) for soil gas monitoring sites on north and south mid-slopes. Small circles indicate sampling depth. Soil pCO_2 values are similar at comparable depths in the planar mid-slopes, but differ significantly ($p = 0.04$) between the swale mid-slopes. Asterisks indicate locations of anomalously high pCO_2 in the soil profiles.

5.3. Variability with depth

While depth is often studied as a control on soil pCO_2, our data show that pCO_2 at the same given depth can vary across a watershed by 100% due to variations in soil moisture. Thus, depth alone will be a weak predictor of the pCO_2 in complex terrain. The observed pattern of increased variance with depth was observed in another study of the montane soils in northeastern Spain (Piñol et al., 1995), where pCO_2 differences were attributed to variations in diffusivity, CO_2 production at various depths in the soil profile, or total CO_2 production over the whole profile.

A minor control on soil pCO_2 in some of our soils (i.e., SPRT, SSMS, SSVF, and NSMS) was the presence of preferential water flowpaths in the soil horizons. Advection of water along the B–C interface is the dominant lateral flow path in the swale, while in the planar transect water advects along both the A–B and B–C interfaces (Lin, 2006; Lin et al., 2006; Jin et al., 2011; Thomas et al., 2013). High soil moisture content along these flowpaths inhibited the diffusive loss of soil pCO_2 to the atmosphere. Thus, while the pCO_2 generally increased with depth, CO_2 was occasionally trapped below these preferential flowpaths, leading to localized CO_2 highs (Figs. 5 and 6; see asterisks).

5.4. Seasonal patterns of soil pCO_2

Seasonality influences soil pCO_2 in the catchment, because time of year governs the soil biological activity and water storage. The seasonal variations in pCO_2 and soil moisture (Figs. S5 and S6) observed in this study are consistent with patterns reported elsewhere (Piñol et al., 1995; Risk et al., 2002; Schulz et al., 2011; Ross et al., 2012). The fall pCO_2 peak is not as large as the peak in June, presumably because lower temperatures limit biological activity (i.e., CO_2 production). Interestingly, the timing of peak pCO_2 at the SSHCZO differs from observations of hillslope soil pCO_2 in the mountainous areas of Montana (Pacific et al., 2008). Pacific et al. (2008) found that during the growing season pCO_2 peaked along a hillslope near the onset of snowmelt (when soil moisture was high) while the highest pCO_2 values in the valley floor occurred later in the summer. We attribute the similarity in timing of peak pCO_2 between topographic positions at SSHCZO to the similar temporal behavior of soil moisture throughout the catchment.

Interestingly, we observed that while the timing of peak soil pCO_2 was similar across the watershed, the amplitude of the pCO_2 peak was higher in the deeper, wetter soils. Because the deeper soils experience the largest seasonal changes in soil moisture (Fig. 3, Figs. S3 and S4), they also experience the largest fluctuations in pCO_2 (Figs. 5 and 6, Figs. S1 and S2). In other words, the ridge top and planar mid-slope soils are more consistently dry throughout the year, and therefore have lower annual variations in pCO_2, while the valley floor and swale soils have more variable soil moisture, and therefore have highly variable pCO_2 levels.

5.5. Implications for weathering

In shallow, well-drained portions of the landscape (i.e., ridge tops and planar hillslopes) the accumulation of CO_2 in the soil profile is substantially lower than in the swales (i.e., the concave portions of the landscape with deep soil profiles), even for the same soil depth due to increased CO_2 diffusion in these shallow soils. We assert that because topography controls soil depth, texture, porosity, and moisture, which all govern soil CO_2 diffusion rates, topographic positions can be used to predict the distribution of soil pCO_2 in watersheds. Moreover, because soil CO_2 dynamics are a key determinant in weathering kinetics, constraining soil pCO_2 variability across topographic positions is needed to understand the distribution of weathering rates across a landscape (Andrews and Schlesinger, 2001). Present-day soil mineral assemblages reflect the residual products of shale bedrock that integrate long-term weathering rates over the entire period of soil development. The short-term weathering rates in the catchment are represented by soil porewater chemistry. At SSHCZO, for example, four observations have been made with respect to weathering that are notable

here: i) the integrated extent of chemical weathering decreases from the ridge top downslope to the valley floor for the south planar transect (Jin et al., 2010), ii) the rate of chemical weathering estimated from porewater chemistry for these three sites does not differ within error (Jin et al., 2011), iii) the integrated extent of chemical weathering in the soil is generally lower for north slope compared to south slope soils (Ma et al., 2011b, 2013), and iv) the chemical weathering rates estimated for the north planar slope soils are faster than for south planar slope soils (Ma et al., 2013). In other words, the integrated extent of chemical weathering increases from the ridge top to the valley floor for the planar slope and is larger for the south slope compared to the north slope, but the instantaneous rate of weathering (as observed in porewater chemistry) does not show these differences.

To understand these observations in the context of soil CO_2, we calculated the pH of porewater in equilibrium with soil CO_2 (Tables S1, S2). For values of 35,000 ppmv (the highest concentration measured during the study period, which occurred at SSMS) the pH of equilibrated porewater is 4.6, substantially lower than the pH of water in equilibrium with atmospheric pCO_2 levels (i.e., rainwater, pH = ~5.6, pCO_2 = ~390 ppmv). In other words, the pH of soil water equilibrated with soil pCO_2 is lower than it would be if it were equilibrated with the atmospheric pCO_2. The porewater pH values, calculated to be in equilibrium with the soil pCO_2, vary by up to 1 pH unit across the catchment (Tables S1 and S2), demonstrating the large variation in weathering potential across the landscape. This is important because the landscape positions with the deepest, wettest soils (i.e., the swale mid-slopes and valley floors) have the highest soil pCO_2. Assuming weathering rates increase with decreasing pH (Brantley, 2008), weathering potential (due to soil pCO_2) might be expected to increase from the ridge top to valley floor and from planar slopes to swales.

Consistent with this, Jin et al. (2010) found that elemental depletion (including Fe, K, Mg, Si, and Al), integrated over the planar hillslope soils, is largest at the valley floor where CO_2 concentrations are highest. Although this enhanced depletion at the valley floor is attributable partly to downslope movement of that material from higher on the hillside as measured by Ma et al. (2010) – and thus longer residence times in the weathering regime – some of the extensive depletion in the valley is likely due to higher pCO_2. However, Jin et al. (2011) could not distinguish a difference in the current rate of weathering at the three landscape positions in the south planar hillslope based on today's soil porewaters. This is consistent with more depleted soils dissolving in a more corrosive porefluid. In other words, although CO_2 is higher in the valley, fewer minerals remain to be weathered.

On the other hand, Jin et al. (2011) also observed low Mg concentrations in porewaters collected from preferential flowpaths, i.e., waters that flushed quickly through the soils. In contrast, Mg concentrations in porewaters increased just below the flowpaths in the low flow zones of the soil. These high Mg porewater concentrations indicate enhanced weathering due to longer water residence times, and coincide with zones where CO_2 is trapped below the wetter flowpaths due to lower diffusion rates (i.e., localized pCO_2 maxima). In this respect, the high CO_2 zones correlate with zones where weathering is ongoing today.

Our results could indicate the potential for a positive feedback between weathering and landscape position: deep, wet soils in swales and valleys have higher weathering potential from CO_2 because CO_2 is trapped by low diffusion due to high soil moisture. This process could amplify variation in weathering across landscapes over time: locations with higher pCO_2 weather more, thus increasing soil depths, leading to higher water content, which allows further accumulation of CO_2. Specifically, rates of chemical weathering in swales are likely to be faster than along planar slopes due to higher pCO_2.

6. Conclusions

Using a topographically explicit pCO_2 sampling regime, we show that the concentration and distribution of soil CO_2 vary significantly between hillslope catena positions, north and south aspects, and planar and swale slopes. Understanding the relative controls of environmental variables on the heterogeneity of soil CO_2 through space and time is critical for predicting changes in soil CO_2 dynamics with respect to regolith weathering. It is well known that soil depth, texture, porosity, moisture, vegetation, and local microbial communities can dramatically influence CO_2 diffusion and production. Depth in particular is often studied as a control on pCO_2; however, our data show that soils from the same depth within a watershed can vary by almost 7-fold in pCO_2. So, depth alone is a weak predictor of pCO_2 in complex terrain.

Topographic position, on the other hand, is a strong predictor of soil depth, texture, porosity, and moisture, and our observations show the importance of landscape position for CO_2 concentrations. Moreover, soil pCO_2 influences porewater pH, and we calculated that the variability in soil pCO_2 observed in the SSHCZO watershed can lead to porewater pH differences of up to 1 pH unit. Thus, topography could improve models of soil CO_2 weathering capacity across landscapes since there are consistent pCO_2 patterns across remotely mappable topographic positions. For example, existing soils maps could be used to distinguish shallow and well-drained portions of the landscape (planar slopes and ridge tops) from deeper, water accumulating portions of the landscape to scale up predictions of soil pCO_2 and associated weathering rates. Slope aspect also controls soil CO_2 distribution, and south (north-facing) swales with deep soils have higher pCO_2 than their north (south-facing) counterparts. We also observed that effect of seasonality on soil pCO_2 varies with topographic position: the annual variability of pCO_2 was larger in the deep, wet soils compared to the shallow, dry soils. These topographic observations will allow us to constrain soil pCO_2 dynamics and, eventually, predict CO_2 dynamics at the watershed-scale using topographic and soil depth maps. Our observations also show that the greatest chemical weathering potential from CO_2 dissolution into porewater occurs in the deeper soils of swales and valleys.

Acknowledgments

We thank those who helped with field work and laboratory analyses, especially Nicholas Kaiser, Daniel Mizsei, and Brian Creamer. Valuable discussions and suggestions provided by Julie Weitzman, Danielle Andrews, Pamela Sullivan, and Forrest Williams during the preparation of the manuscript are greatly appreciated. Jeremy Fine is thanked for his help with constructing figures. We conducted this research at the Penn State Stone Valley Forest, which is funded by The Pennsylvania State University College of Agriculture Sciences, Department of Ecosystem Science and Management and managed by the staff of the Forestlands Management Office. Financial support was provided by National Science Foundation (NSF) grants EAR – 0725019 (Chris Duffy), EAR – 1239285 (Susan Brantley), and EAR – 1331726 (Susan Brantley) for the Susquehanna Shale Hills Critical Zone Observatory. Logistical support and data were provided by the NSF-supported Susquehanna Shale Hills Critical Zone Observatory. We thank two anonymous reviewers who provided constructive comments that helped us improve the manuscript.

Appendix A. Supplementary material

Supplementary material related to this article can be found at http://dx.doi.org/10.1016/j.apgeochem.2015.07.005.

References

Akaike, H., 1974. A new look at the statistical model identification. IEEE Trans. Automat. Control 19, 716–723.

Andrews, D.M., 2011. Coupling Dissolved Organic Carbon and Hydropedology in the Shale Hills Critical Zone Observatory (Ph.D. thesis). The Pennsylvania State University.

Andrews, D.M., Lin, H., Zhu, Q., Jin, L., Brantley, S.L., 2011. Hot spots and hot moments of dissolved organic carbon export and soil organic carbon storage in the Shale Hills catchment. Vadose Zone J. 10, 943–954.

Andrews, J.A., Schlesinger, W.H., 2001. Soil CO_2 dynamics, acidification, and chemical weathering in a temperate forest with experimental CO_2 enrichment. Glob. Biogeochem. Cycles 15, 149–162.

Beaulieu, E., Godderis, Y., Labat, D., Roelandt, C., Oliva, P., Guerrero, B., 2010. Impact of atmospheric CO_2 levels on continental silicate weathering. Geochem. Geophys. Geosyst. 11, 1–18.

Benstead, J., Lloyd, D., 1996. Spatial and temporal variations of dissolved gases (CH_4, CO_2, and O_2) in peat core. Microb. Ecol. 31, 57–66.

Berg, T.M., Edmunds, W.E., Geyer, A.R., et al., 1980. Geologic Map of Pennsylvania. Pennsylvania Geological Survey, Harrisburg, PA, 4th Ser., Map. 1.

Berner, E.K., Berner, R.A., 1996. Global Environment: Water, Air and Geochemical Cycles. Prentice-Hall, Inc., Upper Saddle River, New Jersey.

Brantley, S.L., 2008. Kinetics of mineral dissolution. In: Brantley, S.L., Kubicki, J.D., White, A.F. (Eds.), Kinetics of Water-rock Interaction. Springer-Kluwer, New York.

Brantley, S.L., Lebedeva, M., Bazilevskaya, E., 2013. Relating weathering fronts for acid neutralization and oxidation to pCO_2 and pO_2. In: Farquhar, J., Kasting, J., Canfield, D. (Eds.), Treatise of Geochemistry, the Atmosphere – History. Elsevier, Amsterdam, The Netherlands.

Burton, D.L., Beauchamp, E.G., 1994. Profile nitrous oxide and carbon dioxide concentrations in a soil subject to freezing. Soil Sci. Soc. Am. J. 58, 122–155.

Buyanovsky, G.A., Wagner, G.H., 1983. Annual cycles of carbon dioxide in soil air. Soil Sci. Soc. Am. J. 47, 1140–1145.

Cerling, T.E., 1984. The stable isotopic composition of modern soil carbonate and its relationship to climate. Earth Planet. Sci. Lett. 71, 229–240.

Davidson, E.A., Verchot, L.V., Cattânio, J.H., Ackerman, I.L., Carvalho, J.E.M., 2000. Effects of soil water content on soil respiration in forests and cattle pastures of eastern Amazonia. Biogeochemistry 48, 53–69.

de Jong, E., Schappert, H.J.V., 1972. Calculation of soil respiration and activity from CO_2 profiles in the soil. Soil Sci. 113, 328–333.

Delwiche, L.D., Slaughter, S.J., 2003. The Little SAS Book: a Primer, third ed. Systems Seminar Consultants, Wisconsin, USA.

Eissenstat, D., Wubbles, J., Adams, T., Osborne, J., 2013. Susquehanna Shale Hills Critical Zone Observatory Tree Survey (2008). Integr. Earth Data Appl. http://dx.doi.org/10.1594/IEDA/100268. Cited 26.07.13.

Fierer, N., Chadwick, O.A., Trumbore, S.E., 2005. Production of CO_2 in soil profiles of a California annual grassland. Ecosystems 8, 412–429.

Fisher, D.W., Thorstenson, D.C., Croft, M.G., Houghton, R.L., 1985. Geochemical Processes in the Gascoyne Lignite Mining Area, Bowman County, North Dakota. U.S. Geological Survey, Reston, Virginia, pp. 84–4192. Water-Resources Investigation Report.

Hamada, Y., Tanaka, T., 2001. Dynamics of carbon dioxide in soil profiles based on long-term field observation. Hydrol. Process. 15, 1829–1845.

Jin, L., Andrews, D.M., Holmes, G.H., Lin, H., Brantley, S.L., 2011. Opening the "black box": water chemistry reveals hydrological controls on weathering in the Susquehanna Shale Hills Critical Zone Observatory. Vadose Zone J. 10, 928–942.

Jin, L., Brantley, S.L., 2011. Soil chemistry and shale weathering on a hillslope influenced by convergent hydrologic flow regime at the Susquehanna/Shale Hills Critical Zone Observatory. Appl. Geochem. 26, S51–S56.

Jin, L., Ogrinc, N., Yesavage, T., Hasenmueller, E.A., Ma, L., Sullivan, P.L., Kaye, J.P., Duffy, C., Brantley, S.L., 2014. The CO_2 consumption potential of gray shale weathering: insights from the evolution of carbon isotopes in the Susquehanna Shale Hills critical zone observatory. Geochim. Cosmochim. Acta 142, 260–280.

Jin, L., Ravella, R., Ketchum, B., Bierman, P.R., Heaney, P., White, T.S., Brantley, S.L., 2010. Mineral weathering and elemental transport during hillslope evolution at the Susquehanna/Shale Hills Critical Zone Observatory. Geochim. Cosmochim. Acta 74, 3669–3691.

Kaye, J.P., Hart, S.C., 1998. Restoration and canopy-type effects on soil respiration in a ponderosa pine-bunchgrass ecosystem. Soil Sci. Soc. Am. J. 62, 1062–1072.

Kutz, M., 2006. Mechanical Engineers' Handbook, third ed. John Wiley & Sons, Inc., New York, New York.

Law, B.E., Thornton, P.E., Irvine, J., Anthoni, P.M., Van Tuyl, S., 2001. Carbon storage and fluxes in ponderosa pine forests at different developmental stages. Glob. Change Biol. 7, 755–777.

Lin, H.S., 2006. Temporal stability of soil moisture spatial pattern and subsurface preferential flow pathways in the Shale Hills Catchment. Vadose Zone J. 5, 317–340.

Lin, H.S., Kogelmann, W., Walker, C., Bruns, M.A., 2006. Soil moisture patterns in a forested catchment: a hydropedological perspective. Geoderma 131, 345–368.

Ma, L., Chabaux, F., Pelt, E., Blaes, E., Jin, L., Brantley, S., 2010. Regolith production rates calculated with uranium-series isotopes at the Susquehanna/Shale Hills Critical Zone Observatory. Earth Planet. Sci. Lett. 297, 211–225.

Ma, L., Chabaux, F., West, N., Kirby, E., Jin, L., Brantley, S.L., 2013. Regolith production and transport in the Susquehanna Shale Hills Critical Zone Observatory, part 1: insights from U-series isotopes. J. Geophys. Res. Earth Surf. 118, 722–740.

Ma, L., Jin, L., Brantley, S.L., 2011a. Geochemical behaviors of different element groups during shale weathering at the Susquehanna/Shale Hills Critical Zone Observatory. Appl. Geochem. 26, S89–S93.

Ma, L., Jin, L., Brantley, S.L., 2011b. How mineralogy and slope aspect affect REE release and fractionation during shale weathering in the Susquehanna/Shale Hills Critical Zone Observatory. Chem. Geol. 290, 31–49.

Møldrup, P., Olesen, T., Komatsu, T., Yoshikawa, S., Schjønning, P., Rolston, D.E., 2003. Modeling diffusion and reaction in soils: X. A unifying model for solute and gas diffusivity in unsaturated soil. Soil Sci. 168, 321–337.

Naithani, K.J., Baldwin, D.C., Gaines, K.P., Lin, H., Eissenstat, D.M., 2013. Spatial distribution of tree species governs the spatio-temporal interaction of leaf area index and soil moisture across a forested landscape. PLoS One 8, e58704.

Oh, N.H., Kim, H.S., Richter Jr., D.D., 2005. What regulates soil CO_2 concentrations? A modeling approach to CO_2 diffusion in deep soil profiles. Environ. Eng. Sci. 22, 38–45.

Oh, N.H., Richter Jr., D.D., 2004. Soil acidification induced by elevated atmospheric CO_2. Glob. Change Biol. 10, 1936–1946.

Pacific, V., McGlynn, B., Riveros-Iregui, D., Welsch, D., Epstein, H., 2008. Variability in soil respiration across riparian-hillslope transitions. Biogeochemistry 91 (1), 51–70.

Piñol, J., Alcañiz, J.M., Rodà, F., 1995. Carbon dioxide efflux and pCO_2 in soils of three *Quercus ilex* montane forests. Biogeochemistry 30, 191–215.

Rao, C.R., 1971. Estimation of variance and covariance components-MINQUE theory. J. Multivar. Anal. 257–275.

Rayment, M.B., Jarvis, P.G., 2000. Temporal and spatial variation of soil CO_2 efflux in a Canadian boreal forest. Soil Biol. Biochem. 32, 35–45.

Risk, D., Kellman, L., Beltrami, H., 2002. Soil CO_2 production and surface flux at four climate observatories in eastern Canada. Glob. Biogeochem. Cycles 16, 69-1–69-12.

Riveros-Iregui, D.A., McGlynn, B.L., Marshall, L.A., Welsch, D.L., Emanuel, R.E., Epstein, H.E., 2011. A watershed-scale assessment of a process soil CO_2 production and efflux model. Water Resour. Res. 47, W00J04.

Ross, C.S., Kaye, J.P., Kaye, M.J., Kurth, V.J., Brimmer, R., Hart, S.C., Fulé, P.Z., 2012. Ecosystem carbon remains low for three decades following fire and constrains soil CO_2 responses to precipitation in southwestern ponderosa pine forests. Ecosystems 15, 725–740.

Schulz, M., 2006. USGS Protocol: Stonestrom Samplers: Nested Vertical Soil Gas Samplers. CZEN: Critical Zone Exploration Network. http://www.czen.org/content/stonestrom-samplers-nested-vertical-soil-gas-samplers (Cited 01.08.08.).

Schulz, M., Stonestrom, D., Von Kiparski, G., Lawrence, C., Masiello, C., White, A., Fitzpatrick, J., 2011. Seasonal dynamics of CO_2 profiles across a soil chronosequence, Santa Cruz, California. Appl. Geochem. 26, S132–S134.

Šimůnek, J., Suarez, D.L., 1993. Modeling of carbon-dioxide transport and production in soil 1. model development. Water Resour. Res. 29 (2), 487–497.

Solomon, D.K., Cerling, T.E., 1987. The annual carbon dioxide cycle in a montane soil: observations, modeling, and implications for weathering. Water Resour. Res. 23, 2257–2265.

Sullivan, B.W., Kolb, T.E., Hart, S.C., Kaye, J.P., Dore, S., Montes-Helu, M., 2008. Thinning reduces soil carbon dioxide but not methane flux from southwestern USA ponderosa pine forests. For. Ecol. Manag. 255, 4047–4055.

Susquehanna Shale Hills Critical Zone Observatory (SSHCZO), 2013. Datasets. http://criticalzone.org/shale-hills/data/datasets (Cited 12.08.13.).

Szramek, K., McIntosh, J.C., Williams, E.L., Kanduc, T., Ogrinc, N., Walter, L.M., 2007. Relative weathering intensity of calcite versus dolomite in carbonate-bearing temperate zone watersheds: carbonate geochemistry and fluxes from catchments within the St. Lawrence and Danube river basins. Geochem. Geophys. Geosyst. 8. Q04002.

Tang, J., Baldocchi, D.D., 2005. Tree photosynthesis modulates soil respiration on a diurnal time scale. Glob. Change Biol. 11, 1298–1304.

Tang, J., Baldocchi, D.D., Qi, Y., Xu, L., 2003. Assessing soil CO_2 efflux using continuous measurements of CO_2 profiles in soils with small solid-state sensors. Agric. For. Meteorol. 118, 207–220.

Tang, J., Misson, L., Gershenson, A., Cheng, W., Goldenstein, A.H., 2005. Continuous measurements of soil respiration with and without roots in a ponderosa pine plantation in the Sierra Nevada Mountains. Agric. For. Meteorol. 132, 212–227.

Thomas, E.M., Lin, H., Duffy, C.J., Sullivan, P.L., Holmes, G.H., Brantley, S.L., Jin, L., 2013. Spatiotemporal patterns of water stable isotope compositions at the Shale Hills Critical Zone Observatory: linkages to subsurface hydrologic processes. Vadose Zone J. Special Sect. Front. Hydropedol. Vadose Zone Res. http://dx.doi.org/10.2136/vzj2013.01.0029.

Williams, E.L., Szramek, K.J., Jin, L., Ku, T.C.W., Walter, L.M., 2007. The carbonate system geochemistry of shallow groundwater-surface water systems in temperate glaciated watersheds (Michigan, USA): significance of open-system dolomite weathering. Geol. Soc. Am. Bull. 119, 515–528.